# Models for Impact Assessment of Wind-Based Power Generation on Frequency Control

Alejandro D. Domínguez-García

**Abstract** This chapter develops a modeling framework for studying the impact of variability and uncertainty in wind-based electricity generation on power system frequency. The focus is on time-scales involving governor response (primary frequency control) and automatic generation control (secondary frequency control). The framework includes models of synchronous generators, wind-based electricity sources, the electrical network, and the automatic generation control system. The framework can be used to study the impact of different renewable penetration scenarios on system frequency performance metrics. In order to illustrate the framework, a simplified model of the Western Electricity Coordinating Council (WECC) system is developed.

## 1 Introduction

Driven by initiatives like the DoE SmartGrid [1], electrical energy systems are undergoing a radical transformation in structure and functionality in a quest to increase efficiency and reliability. Such transformations are enabled by the introduction of new technologies such as advanced communication and control; new loads, such as plug-in hybrid electric vehicles (PHEV); advanced power electronics devices for power-flow control, such as flexible AC transmission systems (FACTS), and integration of new renewable-based electricity generation sources, e.g., wind and solar.

Focusing on renewable-based electricity resources, it has long been acknowledged that deep penetration of these resources poses major challenges in power system operations [2, 3, 4]. For example, the high variability of wind speed not only makes wind-based electricity generation intermittent but presents major difficulties

Alejandro D. Domínguez-García
Department of Electrical Engineering University of Illinois at Urbana Champaign
341 Everitt Laboratory, MC-702, Urbana, IL 61801, USA
e-mail: aledan@ILLINOIS.EDU

in its forecast [5]. Thus, wind-based electricity generation is an additional source of uncertainty that impacts power system operation across different time-scales, i.e., unit commitment, economic dispatch (optimal power flow), automatic generation control (AGC), and governor control. The impact of wind uncertainty has received a great deal of attention in both unit commitment and optimal power flow problems. The impact of wind variability and uncertainty on AGC and governor response for frequency control has received less attention (see [6, 7, 8, 9, 10, 11] and the references therein); thus, the focus of this work.

The AGC system is responsible for maintaining the system frequency and keeping the power exchanges between areas at their schedules by controlling the power settings of the units participating in AGC to follow the load profile throughout the day and account for errors in load forecast. Traditional AGC models available in the literature abstract out the electrical network structure, only consider synchronous generators, and aggregate system loads by treating them as a disturbance [12, 13, 14, 15]. Additionally, to the author's knowledge, there are no AGC system models available in the open literature that include wind-based electricity generation. One might be tempted to extend traditional AGC models by treating wind-based generation as a negative load and subtract it from the actual system load. We believe that it is necessary to take a step back and rethink how AGC systems are to be modeled in order to properly account for the unique features of wind-based generation and its possible impact on system frequency. First, wind variability ramp-down events are not as abrupt as the sudden loss of a conventional generating unit [7]. However, they are not as smooth as load ramp-down daily cycles, especially in the presence of weather fronts that result in high winds (entire wind power plants might shut down in just a few minutes). On the other hand, the time constants associated with wind-based electricity generation can be faster than the daily load cycle time constants [7]. In regards to the effect of the electrical network on AGC, we believe it is necessary to explicitly model it to understand its possible effects on mitigating wind variability. Given a certain amount of wind-based power present in a system, it is clear that the impact on system frequency response will be different depending on where wind-based power is injected in the network. For example, if all the power is injected in the same geographical area, it might be the case that due to network constraints, the conventional units in that area participating in AGC must be the ones compensating for wind-based variability. The network might also have some smoothing effects as it does affect the response of the overall closed-loop system dynamic behavior, which is something that traditional AGC models do not capture. In other words, if we disregard the network, the impact of wind-based variability is felt by the machines right away, whereas this does not happen in reality, i.e., the network acts as a filter.

This work builds on our previous work [16], where we were concerned with studying short-term impact of wind variability on power system dynamics without explicitly accounting for the AGC system. This paper introduces an analytically tractable model for quantifying the impact of wind variability and uncertainty in power system frequency response. This model extends traditional AGC models by explicitly including models for wind-based electricity generation sources, and

the electrical network. The model is formulated by using a nonlinear differential-algebraic equation (DAE) formalism. The differential part includes both the conventional synchronous generating units and the wind-based electricity sources, and the AGC system dynamics. The conventional units are described by a third-order model that includes the mechanical equations of motion and the governor dynamics. Since we are only interested in frequency response, it is appropriate to assume that the voltage regulator and other dynamics within the machine are fast enough compared to the phenomena of interest, justifying the use of this third-orde model. The wind-based electricity resources are modeled as a piecewise linear first-order dynamical system describing the relation between power and wind speed. This piecewise linear model naturally captures the nonlinear nature of wind generator power characteristic. The power settings of synchronous generators participating in AGC (it is assumed that wind-based units do not participate in AGC) are modeled following [14, pp. 352-355]. The algebraic part describes the network electrical behavior using standard power flow equations, but separates the power injection at a node into the contributions of conventional synchronous generating units and wind-based electricity sources.

For the timeframes of interest for AGC (seconds to minutes), we assume that forecast errors are small. Then, the nonlinear DAE model is linearized along a nominal system trajectory that results from wind and load forecasts. Then, by using Kron reduction, it is possible to reduce the resulting linear DAE model to an ordinary differential equation (ODE) model. This ODE model describes how variations around wind and load forecast will affect the system dynamics and therefore the frequency. Following [17], it is assumed that, due to the fact that the system is never in steady-state, the system frequency is not homogenous across the system. Thus, frequency on every bus of the network is defined as the nominal system frequency plus the derivative of the voltage angle with respect to time. Therefore, this model can be used to study the impact of wind variability on frequency across the system, which might be relevant for deep penetration scenarios, e.g., 50% of the total power at any given time is served by wind-based resources. We believe that the model can be useful for understanding fundamental limits on the amount of wind that can be integrated in a power system without violating frequency performance metrics. Additionally, the model can be used to design advanced controls to augment AGC. For example, we envision that within the current hierarchy of frequency response controls comprised of governor control and AGC, it may be possible to introduce an intermediate control, acting faster than AGC but slower than governors, to coordinate groups of coherent generators to smooth the variability of wind-based generation in a particular area of the system where these generators are located.

The remainder of this chapter is organized as follows. Section 2 provides the mathematical models for each of the system components. Section 3 provides the formulation of the system nonlinear DAE model and its linearization along a nominal trajectory. Section 4 illustrates the application of the modeling framework to a simplified Western Electricity Coordinating Council (WECC) model. Concluding remarks are presented in Section 5.

## 2 Model Building Blocks

This section provides the mathematical models of the system components, which are conventional synchronous generating units, renewable-based electricity sources, the network, and the automatic generation control system.

### *2.1 Conventional (Synchronous) Generating Units*

For the time-scales of interest, it is shown in [17] that a nine-state machine model, including models for damper-windings, mechanical equations of motion, exciter, voltage regulator, turbine, and the governor, can be reduced to a three-state model that only includes the mechanical equations and the governor dynamics.

For the $i^{th}$ synchronous machine, let $\delta_i$ [rad] denote the rotor electrical angular position (with respect to a synchronous reference rotating at $\omega_s$ [rad/s]), $\omega_i$ [rad/s] denote the rotor electrical angular velocity, and $P_i$ [pu] denote the turbine power. Let $V_i$ [pu] denote the machine terminal voltage magnitude, and $\theta_i$ [rad] denote the machine terminal voltage angle. Let $P_i^{ref}$ [pu] denote the input to the generating unit control logic. If we neglect the motor changer controller dynamics, $P_i^{ref}$ is just the unit power setting. Then, the machine dynamics can be described by:

$$\frac{d}{dt}\begin{bmatrix}\delta_i\\ \omega_i\\ P_i\end{bmatrix} = \begin{bmatrix}0 & 1 & 0\\ 0 & -\frac{D_i}{M_i} & \frac{1}{M_i}\\ 0 & -\frac{1}{\tau_i R_i \omega_s} & -\frac{1}{\tau_i}\end{bmatrix}\begin{bmatrix}\delta_i\\ \omega_i\\ P_i\end{bmatrix} + \begin{bmatrix}0\\ -\frac{E_i V_i}{M_i X_i}\sin(\delta_i-\theta_i)\\ 0\end{bmatrix} + \\ + \begin{bmatrix}-1\\ \frac{D_i}{M_i}\\ \frac{1}{\omega_s \tau_i R_i}\end{bmatrix}\omega_s + \begin{bmatrix}0\\ 0\\ \frac{1}{\tau_i}\end{bmatrix}P_i^{ref}, \tag{1}$$

where $\omega_s$ [rad/s] is the machine electrical synchronous speed, $D_i$ [s/rad] is a damping coefficient, $M_i$ [s$^2$/rad] is the scaled machine inertia constant, $E_i$ [pu] is the voltage behind reactance (or machine "internal voltage"), $\tau_i$ [s] is the governor time constant, and $R_i$ [pu] is the slope of the machine speed-droop characteristic.

As explained in the next section, the generating unit $i$ power setting $P_i^{ref}$ is a function of the unit base-point generation $P_i^{ed}$ (determined by economic dispatch in intervals of five to fifteen minutes), and also by the AGC system generation allocation to the unit $i^{th}$ to account for deviations in frequency, area power exchange, and load (from the value used in the economic dispatch calculation).

## 2.2 Wind-Based Electricity Sources

For the time-scales of interest, it was shown in [18, 19] that, under normal system operation (no faults in the network or sudden loss of synchronous generators), the most important interaction of wind farms with the system is through the interchange of power. Also in [18, 19], it was shown by using model-order reduction, that i) a low-order dynamical model (up to three states) yields a simple yet accurate description of the relation between wind speed and power generated by a wind turbine, and ii) this model can be extended to also describe the power generated by a group of turbines.

In this work, we follow the ideas above and assume that the power generated by a wind farm can be described by a nonlinear dynamical system. For simplicity of subsequent developments and following [19], we assume that a first-order model suffices (the ideas can be easily extended to higher-order models), and that wind power plants are operated in power factor mode, with unity power factor. Although not explicitly shown, this model can also be easily extended to take into account wind power plant operation in voltage control mode. For the $i^{th}$ wind power plant, let $P_i^w$ be the active power generation, $Q_i^w$ the reactive power generation, and $w_i$ be the representative wind speed of the site where the plant is located. Additionally, following the terminology used for single turbine power characteristics [20], denote by $w_i^c$, $w_i^r$, and $w_i^f$ the wind plant representative cut-in, rated, and cut-out (furling) wind speeds.

Then, plant active and reactive power are respectively given by

$$P_i^w = \phi_i(v_i, w_i) := \begin{cases} 0, & \text{for} \quad w_i < w_I^c, \\ \beta_i(v_i), & \text{for} \quad w_i^c \leq w_i < w_i^r, \\ P_i^r, & \text{for} \quad w_i^r \leq w < w_i^f, \\ 0, & \text{for} \quad w \geq w_f, \end{cases} \tag{2}$$

$$Q_i^w = 0, \tag{3}$$

where $P_i^r$ is a constant (assuming all turbines are operational, this is the plant nameplate power), $\beta_i : \mathbb{R} \mapsto \mathbb{R}^+$, and the evolution of $v_i \in \mathbb{R}$ in (2) described by

$$\dot{v}_i = \alpha_i(v_i, w_i), \tag{4}$$

where $w_i \in \mathbb{R}^+$, and $\alpha_i : \mathbb{R} \times \mathbb{R}^+ \mapsto \mathbb{R}$.

Although not explicitly described in (2) and (4), $w_i$ can be modeled as a stochastic process. Since $\phi(\cdot)$ is a piecewise-defined function, the evolution of $P_i^w$ can be formalized using stochastic hybrid modeling formalisms (see, e.g., [21, 22]).

## 2.3 Network

The electrical network is modeled by the standard power flow equations polar-coordinate formulation. At each node, it is assumed that bus power injections can be due to both synchronous generators and wind-based electricity sources. Loads are modeled as active and reactive power withdraws, and the formulation is general to account for the possibility of having loads at every bus of the network.

For the $i^{th}$ bus, let $V_i$ denote the $i^{th}$ bus voltage magnitude, and let $\theta_i$ denote the bus voltage angle. Let $P_i^s$ and $Q_i^s$ denote active and reactive power injections from the $i^{th}$ synchronous generator, and $P_i^w$ denote active power injections from the $i^{th}$ wind power plant. Finally, let $P_i^d$ and $Q_i^d$ be the active and reactive power demand. The power flows equations are

$$P_i^s + P_i^w - P_i^d = \sum_{k=1}^{n} V_i V_k \big(G_{ik}\cos(\theta_i - \theta_k) + B_{ik}\sin(\theta_i - \theta_k)\big), \tag{5}$$

$$Q_i^s - Q_i^d = \sum_{k=1}^{n} V_i V_k \big(G_{ik}\sin(\theta_i - \theta_k) - B_{ik}\cos(\theta_i - \theta_k)\big), \tag{6}$$

where $G_{ik}$ and $B_{ik}$ are the real and imaginary parts, of the network admittance matrix $(i,k)$ entry respectively. It follows from the model in (1) that $P_i^s$ and $Q_i^s$ are given by

$$P_i^s = \frac{E_i V_i}{X_i}\sin(\delta_i - \theta_i), \tag{7}$$

$$Q_i^s = \frac{E_i V_i}{X_i}\cos(\delta_i - \theta_i) - \frac{V_i^2}{X_i}, \tag{8}$$

whereas the model for $P_i^w$ was given in (2).

## 2.4 Automatic Generation Control System

For automatic generator control (AGC) modeling, it is assumed that there are $m$ different balancing areas within the interconnected system, and within each area, only synchronous generators can participate in AGC. The $i^{th}$ generator participating in AGC will adjust its power setting $P_i^{ref}$ according to the corresponding area control error (ACE) and its ACE participation factor. We follow the AGC model in [14, pp. 352-355], except for the assumption made when deriving (1), where the motor changer controller dynamics were neglected.

Denote by $\mathscr{A} = \{1,2,\ldots,m\}$ the set that indexes all balancing areas. For every $k \in \mathscr{A}$, denote by $\mathscr{A}_k \subset \mathscr{A}$ the set of balancing areas that have tie lines with area $k$. Denote by $P_{kj}$ the actual power interchange between areas $k$ and $j$ (positive for power leaving area $k$), and by $f^k$ the actual frequency of area $k$. Then, ACE for area $k$ is given by

$$ACE_k = -\sum_{j \in \mathscr{A}_k} (P^{kj} - P^{kj}_{sch}) - b_k(f^k - f^{nom}), \tag{9}$$

where $P^{kj}_{sch}$ is the scheduled power interchange between areas $k$ and $j$, $B_k$ is the bias factor for area $k$, and $f^{nom}$ is the system nominal frequency.

Let $\mathscr{B}_{kj}$ be the set of buses in area $k$ with tie lines to buses in area $j$, and $\mathscr{B}_{jk}$ be the set of buses in area $j$ with tie lines to buses in area $k$. Denote by $P_{lm}$ the power flow from bus $l$ to bus $m$. Then, the power exchange between areas $k$ and $j$ is

$$P^{kj} = \sum_{l \in \mathscr{B}_{kj}, m \in \mathscr{B}_{jk}} P_{lm} = \sum_{l \in \mathscr{B}_{kj}, m \in \mathscr{B}_{jk}} V_l V_m \big(G_{lm} \cos(\theta_l - \theta_m) + B_{lm} \sin(\theta_l - \theta_m)\big). \tag{10}$$

Let $\alpha^k_l$ denote the ACE participation factor for the $l^th$ generator in control area $k$, and denote by $\mathscr{G}_k$ the set that indexes all the generators in area $k$. Then the power setting of the $l^{th}$ generator in area $k$ is given by

$$\begin{aligned} \frac{dz_k}{dt} &= ACE_k - \sum_{i \in \mathscr{G}_k} (P^{ed}_i + \alpha^k_i (z_i - \sum_{j \in \mathscr{G}_k} P^{ed}_j) - P^s_i), \\ P^{ref}_l &= P^{ed}_l + \alpha^k_l (z_k - \sum_{j \in \mathscr{G}_k} P^{ed}_j), \end{aligned} \tag{11}$$

with $\sum_{i \in \mathscr{G}_k} \alpha^k_i = 1$, and where $P^s_i = \frac{E_i V_i}{X_i} \sin(\delta_i - \theta_i)$, i.e., power generated by unit $i$. Note that (11) is general enough to also include generators that do not participate in AGC by setting their participation factor to zero, which would result in $P^{ref}_l = P^{ed}_l$.

The area $k$ frequency $f_k$ in (9) can be related to the derivatives of the bus voltage angles as follows. Let $f_i$ be the frequency on bus $i$, then

$$f_i = f^{nom} + \frac{1}{2\pi} \frac{d\theta_i}{dt}, \tag{12}$$

where $\theta_i$ is the $i^{th}$ bus voltage angle [17]. Then, the frequency in area $k$ can be obtained as a weighted linear combination of the frequencies in several buses, i.e.,

$$f^k = \sum_{i \in \mathscr{B}_k} \gamma_i f_i \tag{13}$$

with $\sum_{i \in \mathscr{B}_k} \gamma_i = 1$, where $\mathscr{B}_k$ is the set of buses in area $k$. In the simplest case, if the frequency of a single bus is used in (9), the summation in (13) reduces to a single term.

# 3 System Model

We introduce now a system-level nonlinear differential-algebraic model using the building blocks described in the previous section. We then linearize the differential-algebraic model along a nominal trajectory and use Kron reduction to reduce the differential-algebraic model linearization to a time-varying linear system model.

## *3.1 Nonlinear Differential-Algebraic Model*

The system dynamic behavior can be described by a differential-algebraic equation (DAE). The differential part arises from both the individual synchronous machine dynamics as described in (1), the wind power plants as described in (2) and (4), and the AGC system as described in (9)–(13). The algebraic part results from the power flow equations as described in (5) and (6).

Define the vector of synchronous machine state variables as $x = [x_1',\ x_2', \ldots, x_m']'$, with $x_i = [\delta_i,\ \omega_i,\ T_i]'$; the vector of synchronous machine power settings as $u = [P_1^{ref},\ P_2^{ref}, \ldots, P_n^{ref}]'$; the vector of algebraic variables as $y = [y_1',\ y_2', \ldots, y_n']'$, with $y_i = [\theta_i,\ V_i]'$; the vector of wind-power-plant generation as $p_w = [P_1^w,\ P_2^w, \ldots, P_n^w]'$; the vector of load demands as $p_d = [P_1^d,\ P_2^d, \ldots, P_n^d]'$; the vector of wind-power-plant representative wind speeds as $w = [w_1,\ w_2, \ldots, w_n]'$, and $v = [v_1,\ v_2, \ldots, v_n]'$ the vector of wind power plant internal variables defining plants power output evolution between cut-in and rated speed $\big($see (4)$\big)$. Denote by $p^{sch}$ the vector of scheduled power interchange between areas; let $z = [z_1,\ z_2, \ldots, z_m]'$ be the vector of inputs to the generation allocation logic of the units participating in AGC; and let $p_{ed} = [P_1^{ed},\ P_2^{ed}, \ldots, P_n^{ed}]'$ be the vector that results from the solution to the economic dispatch. Then the system dynamic behavior can be described by

$$\frac{dx}{dt} = f(x,y,u), \tag{14}$$

$$\frac{dz}{dt} = h(x,y,z,p_{sch},p_{ed}), \tag{15}$$

$$u = k(z,p_{ed}), \tag{16}$$

$$\frac{dv}{dt} = \alpha(v,w), \tag{17}$$

$$p_w = \phi(v,w), \tag{18}$$

$$0 = g(x,y,p_d,p_w). \tag{19}$$

The function $f : \mathbb{R}^{3n} \times \mathbb{R}^{2n} \times \mathbb{R}^n \mapsto \mathbb{R}^n$ results from the synchronous generator dynamics as described in (1). The function $h : \mathbb{R}^n \times \mathbb{R}^n \times \mathbb{R}^m \times \mathbb{R}^n \times \mathbb{R}^n \mapsto \mathbb{R}^m$ results from the synchronous generators power settings as described in (9)–(13). For the $j^{th}$ with their power setting scheduled solely based on economic dispatch, it follows that $u_j = P_j^{ed}$. The functions $\alpha : \mathbb{R}^n \times (\mathbb{R}^+)^n \mapsto \mathbb{R}^n$, and $\phi : \mathbb{R}^n \times (\mathbb{R}^+)^n \mapsto \mathbb{R}^n$

result from wind power plant dynamics as described in (2) and (4). The function $g : \mathbb{R}^{3n} \times \mathbb{R}^{2n} \times \mathbb{R}^{n} \mapsto \mathbb{R}^{n}$ results from the network power flow equations.

The formulation in (14)–(19) is made general enough to allow the possibility of having wind power plants, loads, and synchronous generator connected to all the buses in the network. If this is not the case, the dimensions of $x$, $p_w$, and $P_d$ should be modified accordingly as illustrated in an example in Section 4.

## *3.2 Linearized Model*

In the nonlinear DAE model described in (14)–(19), there are two inputs that are subject to uncertainty, which are the load demand vector $p_d$ and the wind-power-plant averaged wind speed vector $w$. These uncertain inputs can be characterized by their forecast $p_d^*$ and $w^*$. For the time-scales of interest, we assume that the forecast error is small and linearize the system in (14)–(19) along a nominal trajectory $(x^*, y^*, u^*, p_w^*)$ that results from the forecasted $p_d^*$ and $w^*$. Since the focus here is on the evolution of the system dynamics in the time elapsed between two economic dispatch calculation, and we assume that the economic dispatch solution $p_{ed}^*$ (as well as the power interchange between areas $p_{sch}^*$) remain constant.

Let $x = x^* + \Delta x$, $y = y^* + \Delta y$, $u = u^* + \Delta u$, $p_w = p_w^* + \Delta p_w$, $w = w^* + \Delta w$, and $p_d = p_d^* + \Delta p_d$. Then, small variations in system trajectories around $(x^*, y^*, u^*, p^*)$ arising from small variations around $p_d^*$ and $w^*$ can be approximated by

$$\frac{d\Delta x}{dt} = A_1(t)\Delta x + A_2(t)\Delta y + B_1(t)\Delta u, \tag{20}$$

$$\frac{d\Delta z}{dt} = A_3(t)\Delta x + A_4(t)\Delta y + A_5(t)\Delta z, \tag{21}$$

$$\Delta u = B_2(t)\Delta z, \tag{22}$$

$$\frac{d\Delta p_w}{dt} = F(t)\Delta p_w + G(t)\Delta w, \tag{23}$$

$$0 = C_1(t)\Delta x + C_2(t)\Delta y + D_1(t)\Delta p_d + D_2(t)\Delta p_w, \tag{24}$$

where:

$A_1(t) = \frac{\partial f(x,y,u)}{\partial x}\big|_{x^*,y^*,u^*}$, $A_2(t) = \frac{\partial f(x,y,u)}{\partial y}\big|_{x^*,y^*,u^*}$, $B_1(t) = \frac{\partial f(x,y,u)}{\partial u}\big|_{x^*,y^*,u^*}$,

$A_3(t) = \frac{\partial h(x,y,p_{sch},p_{ed})}{\partial x}\big|_{x^*,y^*,p_{sch}^*,p_{ed}^*}$, $A_4(t) = \frac{\partial h(x,y,p_{sch},p_{ed})}{\partial y}\big|_{x^*,y^*,p_{sch}^*,p_{ed}^*}$

$A_5(t) = \frac{\partial h(x,y,p_{sch},p_{ed})}{\partial z}\big|_{x^*,y^*,p_{sch}^*,p_{ed}^*}$, $B_2(t) = \frac{\partial k(z,p_{ed})}{\partial z}\big|_{z^*,p_{ed}^*}$,

$C_1(t) = \frac{\partial g(x,y,p_d,p_w)}{\partial x}\big|_{x^*,y^*,p_d^*,p_w^*}$, $C_2(t) = \frac{\partial g(x,y,p_d,p_w)}{\partial y}\big|_{x^*,y^*,p_d^*,p_w^*}$,

$D_1(t) = \frac{\partial g(x,y,p_d,p_w)}{\partial p_d}\big|_{x^*,y^*,p_d^*,p_w^*}$, $D_2(t) = \frac{\partial g(x,y,p_d,p_w)}{\partial p_w}\big|_{x^*,y^*,p_d^*,p_w^*}$,

$F(t) = \mathrm{diag}\big(F_1(t), F_2(t), \ldots, F_n(t)\big)$, $G(t) = \mathrm{diag}\big(G_1(t), G_2(t), \ldots, G_n(t)\big)$,

with

$$F_i(t) = \begin{cases} \frac{\partial \alpha_i(v_i,w_i)}{\partial v_i}\big|_{v_i^*,w_i^*}, & w_i^c \le w_i < w_i^r, \\ 0, & \text{otherwise}, \end{cases} \tag{25}$$

and

$$G_i(t) = \begin{cases} \frac{\partial \beta_i(v_i)}{\partial v_i}\big|_{v_i^*} \frac{\partial \alpha_i(v_i,w_i)}{\partial w_i}\big|_{v_i^*,w_i^*}, & w_i^c \le w_i < w_i^r, \\ 0, & \text{otherwise}. \end{cases} \tag{26}$$

In (24), as long as $C_2(t)$ is invertible, we can solve for $\Delta y$ to obtain

$$\Delta y = -C_2^{-1}(t)\big(C_1(t)\Delta x + D_1(t)\Delta p_d + D_2(t)\Delta p_w\big). \tag{27}$$

A closer look at $C_2(t) = \frac{\partial g(x,y,p_d,p_w)}{\partial y}\big|_{x^*,y^*,p_d^*,p_w^*}$ reveals that $C_2(t)$ is invertible if and only if the power flow Jacobian is invertible. We assume that for the nominal system trajectory $(x^*,y^*,u^*,p^*)$, invertibility of the power flow equations Jacobian always holds. Then, we can use (27) to substitute $\Delta u$ in (20) and (21), and obtain an ordinary differential equation model of the form

$$\frac{d}{dt}\begin{bmatrix} \Delta x \\ \Delta z \\ \Delta p_w \end{bmatrix} = \begin{bmatrix} A_{11}(t) & A_{12}(t) & A_{13}(t) \\ A_{21}(t) & A_{22}(t) & A_{23}(t) \\ A_{31}(t) & A_{32}(t) & A_{33}(t) \end{bmatrix} \begin{bmatrix} \Delta x \\ \Delta z \\ \Delta p_w \end{bmatrix} + \begin{bmatrix} B_{11}(t) & B_{12}(t) \\ B_{21}(t) & B_{22}(t) \\ B_{31}(t) & B_{32}(t) \end{bmatrix} \begin{bmatrix} \Delta w \\ \Delta p_d \end{bmatrix}, \tag{28}$$

where
$A_{11}(t) = A_1(t) - A_2(t)C_2^{-1}(t)C_1(t)$, $A_{12}(t) = B_1(t)B_2(t)$, $A_{13}(t) = -A_2(t)C_2^{-1}(t)D_1(t)$,
$A_{21}(t) = A_3(t) - A_4(t)C_2^{-1}(t)C_1(t)$, $A_{22}(t) = A_5(t)$, $A_{23}(t) = -A_4(t)C_2^{-1}(t)D_2(t)$,
$A_{31}(t) = 0$, $A_{32}(t) = 0$, $A_{33}(t) = F(t)$, $B_{11}(t) = 0$, $B_{12}(t) = -A_2(t)C_2^{-1}(t)D_1(t)$,
$B_{21}(t) = 0$, $B_{22}(t) = -B_2(t)C_2^{-1}(t)D_1(t)$, $B_{31}(t) = G(t)$, $B_{32}(t) = 0$.

## 4 Example

In this section, the modeling ideas presented in the previous section are illustrated with the 3-machine, 6-bus system of Fig. 1, which is an adaption of the 3-machine, 9-bus model of the Western System Coordinating Council (WECC) system [17]. As depicted in Fig. 1, we consider two balancing areas. We also introduce wind power plants at buses 4 and 5. Also depicted in the figure are the frequency and power exchange feedback loops, as well as the generator power setting control loops.

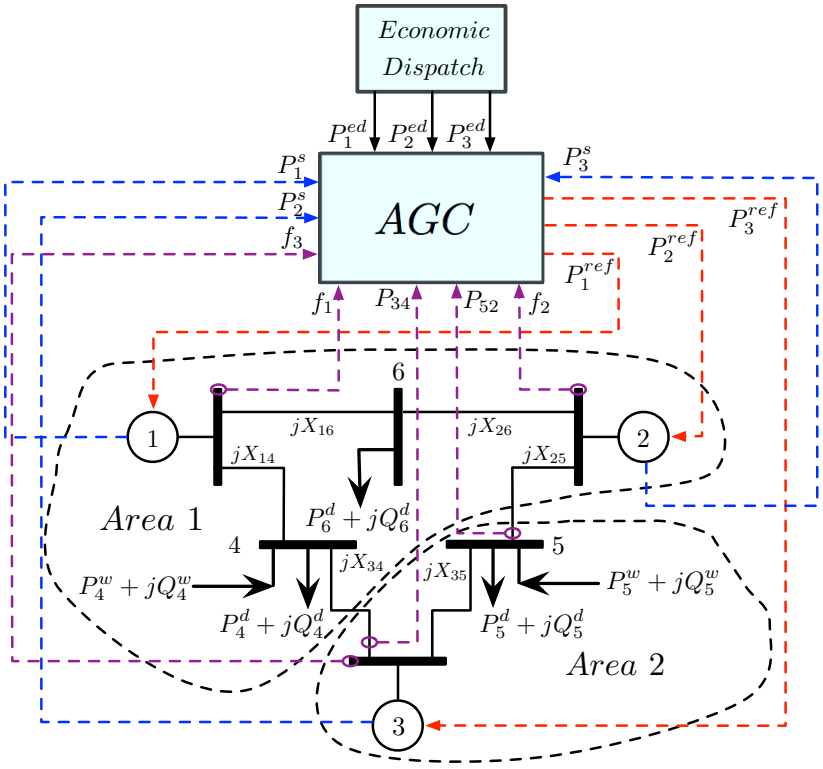


**Fig. 1** 3-machine, 6-bus system with 2 balancing areas.

## *4.1 Dynamics of Conventional (Synchronous) Generating Units*

As described in (14), the dynamics of the synchronous generators in the system can be compactly written as $\frac{dx}{dt} = f(x,y,u)$. In this example, $x = [x_1,\ x_2,\ x_3]'$, with $x_i = [\delta_i,\ \omega_i,\ P_i]'$; $y = [y_1,\ y_2,\ y_3,\ y_4,\ y_5,\ y_6]'$, with $y_i = [\theta_i,\ V_i]'$; and $u = [P_1^{ref},\ P_2^{ref},\ P_3^{ref}]'$, which results in

$$\frac{d}{dt}\begin{bmatrix} x_1 \\ x_2 \\ x_3 \end{bmatrix} = \begin{bmatrix} \Phi_1 & 0 & 0 \\ 0 & \Phi_2 & 0 \\ 0 & 0 & \Phi_3 \end{bmatrix}\begin{bmatrix} x_1 \\ x_2 \\ x_3 \end{bmatrix} + \begin{bmatrix} \Gamma_1(x_1,y_1) \\ \Gamma_2(x_2,y_2) \\ \Gamma_3(x_3,y_3) \end{bmatrix} + \begin{bmatrix} \Upsilon_1 \\ \Upsilon_2 \\ \Upsilon_3 \end{bmatrix} + \begin{bmatrix} \Lambda_1 & 0 & 0 \\ 0 & \Lambda_2 & 0 \\ 0 & 0 & \Lambda_3 \end{bmatrix}\begin{bmatrix} P_1^{ref} \\ P_2^{ref} \\ P_3^{ref} \end{bmatrix}, \tag{29}$$

where

$$\Phi_i = \begin{bmatrix} 0 & 1 & 0 \\ 0 & -\frac{D_i}{M_i} & \frac{1}{M_i} \\ 0 & -\frac{1}{\tau_i R_i \omega_s} & -\frac{1}{\tau_i} \end{bmatrix}, \ \Gamma_i(x_i) = \begin{bmatrix} 0 \\ -\frac{E_i V_i}{M_i X_i} \sin(\delta_i - \theta_i) \\ 0 \end{bmatrix}, \ \Upsilon_i = \begin{bmatrix} -\omega_s \\ \omega_s \frac{D_i}{M_i} \\ \frac{1}{\tau_i R_i} \end{bmatrix}, \ \Lambda_i = \begin{bmatrix} 0 \\ 0 \\ \frac{1}{\tau_i} \end{bmatrix},$$

which is of the form in (14).

## 4.2 Dynamics of Wind Power Plants

As described in (17) and (18), the dynamics of the wind power plants can be compactly written as $\frac{dv}{dt} = \alpha(v,w),\ p_w = \phi(v,w)$. In this example, there are only wind power plants at buses 4 and 5. It is assumed that the wind speed at the location of the wind power plant connected to bus 4 is such that the plant is operating at its rated power. Also, it is assumed that the wind power plant connected to bus 5 is operating between its cut in and rated speeds. Thus $v = [v_4,\ v_5]'$, $p_w = [p_4^w,\ p_5^w]'$, and $w = [w_4,\ w_5]'$, which results in

$$\begin{aligned} \frac{d}{dt}\begin{bmatrix} v_4 \\ v_5 \end{bmatrix} &= \begin{bmatrix} \alpha_4(v_4, w_4) \\ \alpha_5(v_5, w_5) \end{bmatrix}, \\ \begin{bmatrix} P_4^w \\ P_5^w \end{bmatrix} &= \begin{bmatrix} P_4^r \\ \beta_5(v_5, w_5) \end{bmatrix}, \end{aligned} \tag{30}$$

where $P_4^r$ is the nameplate power of the wind power plant connected to bus 4.

## 4.3 Network

As described in (19), the network power flow equations can be compactly written as $0 = g(x,y,p_d,p_w)$. In this example, $p_d = [P_4^d,\ P_5^d, P_6^d]'$, and $p_w = [P_4^w,\ P_5^w]'$. Denote by $Y_{ik} = 1/X_{ik}$ the admittance of the transmission line between buses $i$ and $k$. Then, the power balance equations for bus 1 are

$$\begin{aligned} \frac{E_1 V_1}{X_1} \sin(\delta_1 - \theta_1) =& Y_{14} V_1 V_4 \sin(\theta_1 - \theta_4) + Y_{16} V_1 V_6 \sin(\theta_1 - \theta_6), \\ \frac{E_1 V_1}{X_1} \cos(\delta_1 - \theta_1) - \frac{V_1^2}{X_1} =& - Y_{14} V_1 V_4 \cos(\theta_1 - \theta_4) - Y_{16} V_1 V_6 \cos(\theta_1 - \theta_6) \\ & + (Y_{14} + Y_{16} + Y_1) V_1^2. \end{aligned} \tag{31}$$

The power balance equations for bus 2 are given by

$$\begin{aligned}\frac{E_2V_2}{X_2}\sin(\delta_2-\theta_2) =& Y_{25}V_2V_5\sin(\theta_2-\theta_5)+Y_{26}V_2V_6\sin(\theta_2-\theta_6),\\ \frac{E_2V_2}{X_2}\cos(\delta_2-\theta_2)-\frac{V_2^2}{X_2} =& -Y_{25}V_2V_5\cos(\theta_2-\theta_5)-Y_{26}V_1V_6\cos(\theta_2-\theta_6)\\ &+Y_{25}+Y_{26}+Y_2)V_2^2. \end{aligned} \tag{32}$$

The power balance equations for bus 3 are given by

$$\begin{aligned}\frac{E_3V_3}{X_3}\sin(\delta_3-\theta_3) =& Y_{34}V_3V_4\sin(\theta_3-\theta_4)+Y_{35}V_3V_5\sin(\theta_3-\theta_5),\\ \frac{E_3V_3}{X_3}\cos(\delta_3-\theta_3)-\frac{V_3^2}{X_3} =& -Y_{34}V_3V_4\cos(\theta_3-\theta_4)-Y_{35}V_3V_5\cos(\theta_3-\theta_5)\\ &+(Y_{34}+Y_{35}+Y_3)V_3^2. \end{aligned} \tag{33}$$

The power balance equations for bus 4 are given by

$$\begin{aligned}P_4^w-P_4^d &= Y_{14}V_4V_1\sin(\theta_4-\theta_1)+Y_{34}V_4V_3\sin(\theta_4-\theta_3),\\ Q_4^w-Q_4^d &= -Y_{14}V_4V_1\cos(\theta_4-\theta_1)-Y_{34}V_4V_3\cos(\theta_4-\theta_3)+(Y_{14}+Y_{34})V_3^2. \end{aligned} \tag{34}$$

The power balance equations for bus 5 are given by

$$\begin{aligned}P_5^w-P_5^d &= Y_{25}V_5V_2\sin(\theta_5-\theta_2)+Y_{35}V_5V_3\sin(\theta_5-\theta_3),\\ Q_5^w-Q_5^d &= -Y_{25}V_5V_2\cos(\theta_5-\theta_2)-Y_{35}V_5V_3\cos(\theta_5-\theta_3)+(Y_{25}+Y_{35})V_5^2. \end{aligned} \tag{35}$$

The power balance equations for bus 6 are given by

$$\begin{aligned}-P_6^d &= Y_{16}V_6V_1\sin(\theta_6-\theta_1)+Y_{26}V_6V_2\sin(\theta_6-\theta_2),\\ -Q_6^d &= -Y_{16}V_6V_1\cos(\theta_6-\theta_1)-Y_{26}V_6V_2\cos(\theta_6-\theta_2)+(Y_{16}+Y_{26})V_6^2. \end{aligned} \tag{36}$$

### *4.4 Automatic Generation Control*

The AGC block diagram for this example is depicted in Fig. 2. As described in (15) and (16) , the power settings of generators participating in AGC can be compactly written as $\frac{du}{dt} = h(x,y,p_{sch},p_{ed}),\ u = k(z,p_{ed})$. In this example $u = [P_1^{ref},\ P_2^{ref},\ P_3^{ref}]'$. For area 2, we assume that the frequency measurement used in the ACE is the average of the frequencies on buses 1 and 3. Thus, the power setting of generators 1 and 2 in balancing area 1 are given by

$$
\begin{aligned}
ACE_1 =& -(P^{12} - P^{12}_{sch}) - b_1(f^1 - f^{nom}),\\
P^{12} =& P_{43} + P_{25} = Y_{34}V_4V_3\sin(\theta_4 - \theta_3) + Y_{25}V_2V_5\sin(\theta_2 - \theta_5),\\
\frac{dz_1}{dt} =& ACE_1 - \left[P^{ed}_1 + \alpha^1_1\left(z_1 - (P^{ed}_1 + P^{ed}_2)\right) - P^s_1\right]\\
&+ \left[P^{ed}_2 + \alpha^1_2\left(z_1 - (P^{ed}_1 + P^{ed}_2)\right) - P^s_2\right], \qquad (37)\\
P^{ref}_1 =& P^{ed}_1 + \alpha^1_1\left(z_1 - (P^{ed}_1 + P^{ed}_2)\right),\\
P^{ref}_2 =& P^{ed}_2 + \alpha^1_2\left(z_1 - (P^{ed}_1 + P^{ed}_2)\right), \qquad (38)
\end{aligned}
$$

where $f^1 = \frac{f_1+f_3}{2}$. The frequencies in buses 1 and 3 can be related to the voltage angles in buses 1 and 3 as follows:

$$
\begin{aligned}
f_1 &= f^{nom} + \frac{1}{2\pi}\frac{d\theta_1}{dt},\\
f_2 &= f^{nom} + \frac{1}{2\pi}\frac{d\theta_2}{dt}. \qquad (39)
\end{aligned}
$$

For area 2, we assume that the frequency used in the ACE is the frequency on bus 6. Thus the power setting of generator 3 in balancing area 2 is given by

$$
\begin{aligned}
&ACE_2 = -(P^{21} - P^{21}_{sch}) - b_2(f^2 - f^{nom}),\\
&P^{12} = P_{34} + P_{52} = Y_{34}V_3V_4\sin(\theta_3 - \theta_4) + Y_{25}, V_5V_2\sin(\theta_5 - \theta_2)\\
&\frac{dz_2}{dt} = ACE_2 - \left[P^{ed}_3 + \alpha^2_3\left(z_2 - P^{ed}_3\right) - P^s_3\right],\\
&P^{ref}_3 = P^{ed}_3 + \alpha^2_3\left(z_2 - P^{ed}_3\right) - P^s_3 \qquad (40)
\end{aligned}
$$

where $f^2 = f_3$, and $\alpha^2_3 = 1$. By rearranging (38) and (40), we obtain an expression of the form in (15) and (16).

## 5 Concluding Remarks

This chapter developed a dynamical model for capturing the impact of deep penetration of wind resources on system frequency response. This model includes the electrical network, which in AGC models is usually suppressed. Our hypothesis is that, for deep penetration scenarios, the network may also have some substantial smoothing effects as it does affect the response of the overall closed-loop system dynamic behavior. We believe that the model can be useful for understanding fundamental limits on the amount of wind that can be integrated in a power system without violating frequency performance metrics. Future work will include the comparison of the behavior of this model and classical models available in the literature to verify whether or not our hypothesis is indeed correct or on the contrary, the effect of the network to smooth out wind variability can be neglected.

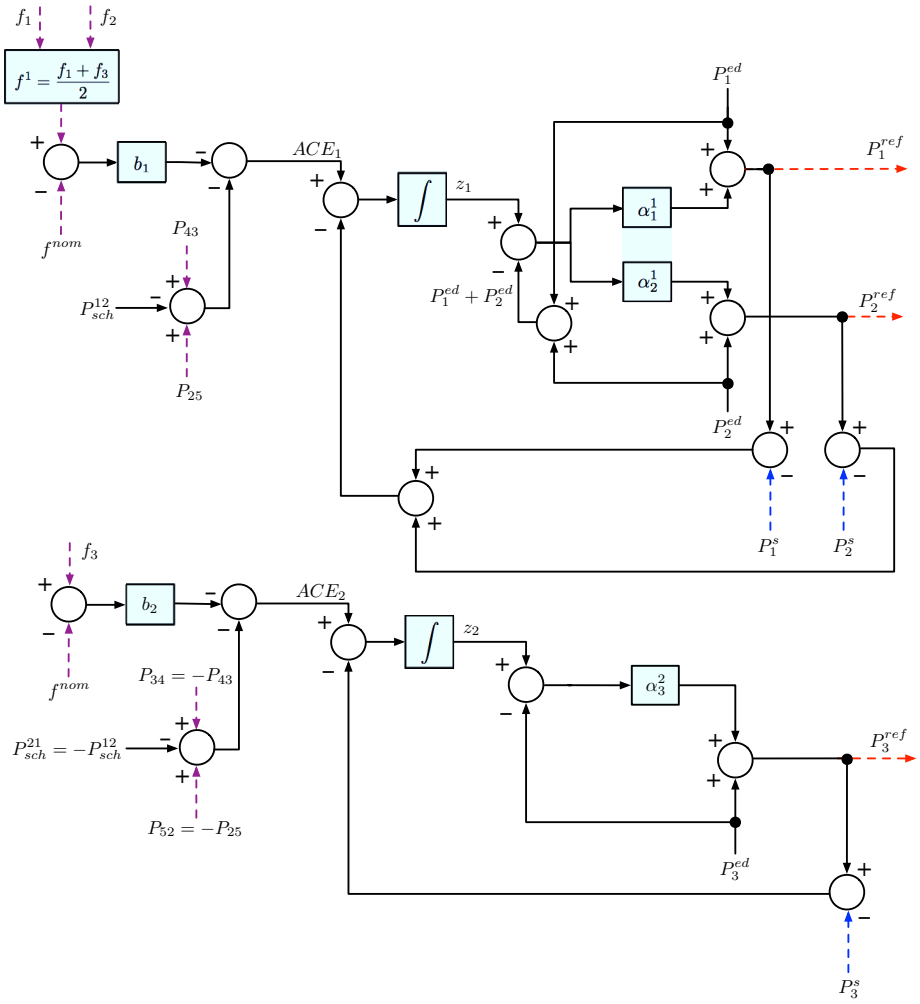


**Fig. 2** AGC system for 3-machine, 6-bus system.

**Acknowledgements** This work has been supported by the Global Climate and Energy Project. Any opinions, findings, and conclusions or recommendations expressed in this publication are those of the author and do not necessarily reflect the views of Stanford University, the Sponsors of the Global Climate and Energy Project, or others involved with the Global Climate and Energy Project.

## References


1. U. S. Department of Energy . The smart grid: an introduction. [Online]. Available: http://www.oe.energy.gov/smartgrid.htm
2. E. Hirst, "Integrating wind output with bulk power operations and wholesale electricity markets," *Wind Energy*, vol. 5, no. 1, pp. 19–36, 2002.
3. P. Eriksen, T. Ackermann, H. Abildgaard, P. Smith, W. Winter, and J. R. Garcia, "System operation with high wind penetration," *IEEE Power and Energy Magazine*, vol. 3, no. 6, pp. 65–74, Nov.-Dec. 2005.
4. E. DeMeo, G. Jordan, C. Kalich, J. King, M. Milligan, C. Murley, B. Oakleaf, and M. Schuerger, "Accommodating wind's natural behavior," *IEEE Power and Energy Magazine*, vol. 5, no. 6, pp. 59–67, Nov.-Dec. 2007.
5. M. Ahlstrom, L. Jones, R. Zavadil, and W. Grant, "The future of wind forecasting and utility operations," *IEEE Power and Energy Magazine*, vol. 3, no. 6, pp. 57–64, Nov.-Dec. 2005.
6. J. Eto *et al.*, "Use of frequency response metrics to assess the planning and operating requirements for reliable integration of variable renewable generation," Lawrence Berkeley National Laboratory, Tech. Rep. LBNL-4142E, December 2010.
7. J. Undrill, "Power and frequency control as it relates to wind-powered generation," Lawrence Berkeley National Laboratory, Tech. Rep. LBNL-4143E, December 2010.
8. C. Martinez, S. Xue, and M. Martinez, "Review of the recent frequency performance of the eastern, western and ercot interconnections," Lawrence Berkeley National Laboratory, Tech. Rep. LBNL-4144E, December 2010.
9. H. Illian, "Frequency control performance measurement and requirements," Lawrence Berkeley National Laboratory, Tech. Rep. LBNL-4145E, December 2010.
10. P. Mackin *et al.*, "Dynamic simulations studies of the frequency response of the three u.s. interconnections with increased wind generation," Lawrence Berkeley National Laboratory, Tech. Rep. LBNL-4146E, December 2010.
11. K. Coughlin and J. Eto, "Analysis of wind power and load data at multiple time scales," Lawrence Berkeley National Laboratory, Tech. Rep. LBNL-4147E, December 2010.
12. A. Debs, Ed., *Modern Power Systems Control and Operation*. Boston, MA: Kluwer Academic Publishers, 1988.
13. P. Kundur, *Power system stability and control*. New York, NY: McGraw Hill Inc, 1994.
14. A. Wood and B. Wollenberg, Eds., *Power Generation, Operation, and Control*. New York, NY: Wiley, 1996.
15. M. Ilic and J. Zaborzky, Eds., *Dynamics and Control of Large Electric Power Systems*. New York, NY: Wiley, 2000.
16. Y. C. Chen and A. Domímguez-García, "Assessing the impact of wind variability on power system small-signal reachability," in *Proc. Hawaii International Conference on System Sciences*, Jan. 2011.
17. P. Sauer and A. Pai, *Power System Dynamics and Stability*. Upper Saddle River, NJ: Prentice Hall, 1998.
18. H. Pulgar, "Wind farm model for power system stability analysis," Ph.D. dissertation, University of Illinois at Urbana-Champaign, Urbana, IL, 2010.
19. H. A. Pulgar-Painemal, "Towards a wind farm reduced-order model," *Electric Power Systems Research*, vol. In Press, Corrected Proof, 2011.
20. T. Ackermann, *Wind Power in Power Systems*. Chichester, UK: John Wiley and Sons, 2005.
21. J. Hespanha, "A model for stochastic hybrid systems with application to communication networks," *Nonlinear Analysis,* Special Issue on Hybrid Systems, vol. 62, no. 8, pp. 1353–1383, Sep. 2005.
22. ——, "Modeling and analysis of stochastic hybrid systems," *IEE Proc. Control Theory and Applications, Special Issue on Hybrid Systems*, vol. 153, pp. 520–535, 2007.